Estimation of the Heat Flux Parameters : Application to GTA Static Welding Spot

Sreedhar Unnikrishnakurup, Sébastien Rouquette, Fabien Soulié, Gilles Fras

4th Inverse Problems, Design and Optimization Symposium (IPDO-2013)
Albi, France, June 26-28, 2013

ESTIMATION OF THE HEAT FLUX PARAMETERS: APPLICATION TO GTA STATIC WELDING SPOT

Sreedhar Unnikrishnakurup, Sebastien Rouquette, Fabien Soulie, Gilles Fras
Laboratoire de Mecanique et Génie Civil, LMGC-UMR 5508, Université de Montpellier 2, CC048, Place Eugène Bataillon, 34095 Montpellier Cédex 05, France, sebastien.rouquette@univ-montp2.fr.

Abstract

A numerical magneto-thermo-hydrodynamic (MTHD) model coupled with an inverse optimization method is developed for the identification of heat flux parameters for the Gas Tungsten Arc Welding (GTAW) process. The MTHD model is based on the four conservation equations of mass, momentum (Navier-Stokes equations), energy (heat transfer) and electric potential. The stated MTHD includes the force term due to magnetic field in the momentum equation (Lorentz force). The transport phenomena and the heat transfer from the electrical arc plasma to the weld pool determine the weld penetration and the weld pool shape. In the current study an attempt has been made to replace the argon electrical arc plasma effect with a heat flux modelled by a Gaussian function on the anode surface. The major parameters that influence the formation of weld pool shape were identified using a parametric study and are welding efficiency and base radius of the Gaussian distribution. A multivariable optimization algorithm based on Levenberg-Marquardt Method is used for the inverse problem. It is concluded that algorithm developed were able to predict the reference numerical model and demonstrated the stability and robustness of the algorithm using a noised input data.

Nomenclature

A_γ	Surface tension gradient constant (N/m/K)	$B_\theta(r,z)$	Azimuthal magnetic field (T)
f_{liq}	Liquid fraction	$I_S(t)$	Welding intensity (A)
$\boldsymbol{J}=(J_r,J_z)$	Current density vector (A/m^2)	Q_J	Joule heating source (W/m^3)
r,z	Spatial variables (m)	R_g	Gas constant (J/kg/mol/K)
$S(p)$	Objective function	T	Temperature (K)
$\boldsymbol{V}=(u,w)$	Velocity vector (m/s)	$\gamma(T,a_S)$	Surface tension coefficient (N/m)
γ_m	Surface tension coefficient for pure metal (N/m)	μ_0	Magnetic constant (T.m/A)
σ_E	Electric resistivity (Ω/m)	τ_{ARC}	Arc shear stress (N/m)
$\varphi(r,z,t)$	Gaussian heat flux (W/m^2)	$\phi(r,z)$	Electric potential (V)
ΔH_0	Standard heat of adsorption (J/kg/mol)	ΔH_f	Latent heat of fusion (J/kg)

Introduction

Gas Tungsten Arc Welding (GTAW) is a joining process that involves the phase change of materials. This process is widely used in many engineering applications where excellent joint quality is required such as aerospace, automotive, nuclear, petro-chemical and ship building industries. Many researchers carried out tremendous amount of work in understanding the basic phenomena occurring in the arc welding process [1-6].

Simulation tools based on finite element method are very useful in the prediction of temperature and velocity fields in fusion zone. Owing to the growing needs of automation and better weld quality control there have been several attempts to model the actual welding phenomena by considering all the physics involved in the weld pool [6]. All these models require the specification of net thermal input from the welding arc to the work piece along with its spatial distribution. The research on welding heat source models dates back 1940s and Rosenthal [7] first proposed a mathematical model of the moving heat

source under the assumptions quasi-stationary state and concentrated point heating in the 3D analysis. In the late 1960s, Pavelic et al. [8] suggested a circular disc heat source model with Gaussian distribution of heat flux on the surface of work piece. Goldak et al. [9] further developed a double ellipsoidal power density distribution of heat source model below the welding arc, which can accurately simulate different type of welding processes with shallow and deep penetration. These heat source models and some simplified models have been widely used in welding simulation for prediction of temperature field, distortion and the residual stresses [10]. In the current study to simulate the heat flux from the arc we used the Gaussian heat distribution because of the consideration that less heat flux penetration is involved in arc welding process than the high power density welding processes(EBW and LBW), where the double ellipsoidal model can capture the flux penetration effectively.

The inverse modeling of welding heat transfer involves finding the parameters such as heat flux, material property, liquid/solid interface; … from the knowledge of the thermal histories and/or weld pool size (with macrographs) [11-14]. Many of the welding variables such as welding current, voltage, speed, and material properties are known with some reasonable degree accuracy. In contrast for the arc welding such as Tungsten Inert Gas welding(TIG), the parameters such as arc efficiency, arc radius, the effective thermal conductivity and the effective viscosity of the molten metal cannot always assigned easily [11-13]. In the current study an attempt has been made to develop a modeling procedure using the 2D-axisymmetric numerical model to calculate the optimum values of some of the unknown variables that mentioned above. The optimization algorithm used for the parameter estimation was Levenberg-Marquardt Method (LMM). The Levenberg-Marquardt technique is widely used for the estimation of optimum single values of several unknown parameters and involves optimization of variables by nonlinear least square technique [15].

1. Formulation of direct problem

1.1 Mathematical Model

The computational model for the current study is limited to the anode. The multi-physics problem comprises of electromagnetism, fluid flow and heat transfer as shown in figure 1. The molten weld pool and the different forces considered for the current study is also represented in Figure 1.

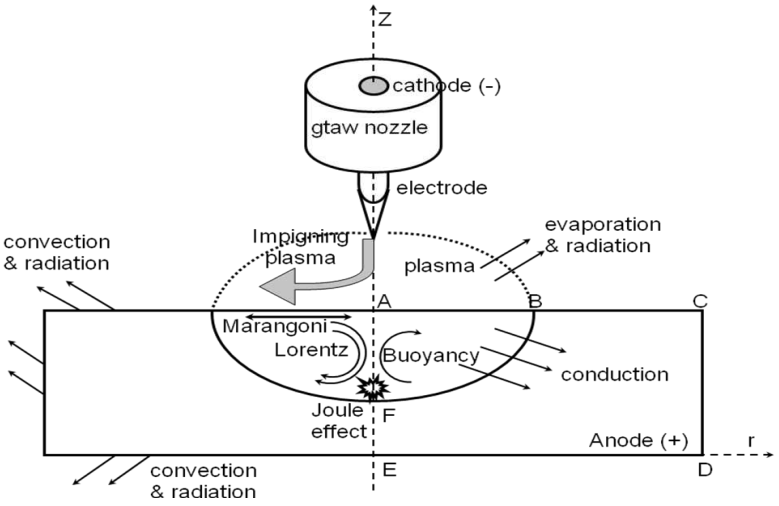

Figure 1: Schematic of transport phenomena occuring in the GTA Welding process

The following major assumptions were made:

1. Static TIG welding (the arc is stationary) is carried out and the 2D-axisymmetric model is assumed.
2. Molten metal flow in the weld pool is considered as laminar and incompressible due to the small size of the weld pool.

3. Buoyancy force is taken into account using the Boussinesq approximation [16], and the latent heat of fusion is taken into account.
4. The surface tension coefficient is dependent on both temperature and sulfur content of the alloy using the Sahoo et al. [17] relationship.
5. A flat weld pool surface is considered.
6. A spatially distributed heat flux, current and arc drag force falling on the free surface are Gaussian characteristics.

Based on the above assumptions, the classical incompressible Navier-Stokes equations for a Newtonian viscous fluid must be considered to get the velocity, pressure and temperature fields.
Mass conservation:

$$\nabla \cdot \mathbf{V} = \frac{1}{r}\frac{\partial (ru)}{\partial r} + \frac{\partial w}{\partial z} = 0 \tag{1}$$

Momentum conservation:

$$\rho \frac{\partial \mathbf{V}}{\partial \mathbf{t}} + \rho(\mathbf{V}.\nabla)\mathbf{V} = -\nabla p + \nabla \cdot \mu \nabla \mathbf{V} + \mathbf{S_u} \tag{2}$$

Energy conservation:

$$\rho c_p^{eq} \frac{\partial T}{\partial t} + \rho c_p^{eq} \mathbf{V} \nabla T = \nabla \cdot (k \nabla T) + S_T \tag{3}$$

Where p is pressure, μ is viscosity and S_u represents the body forces in the weld pool, it is the sum of buoyancy force and Lorentz force it can be expressed as:

$$\mathbf{S_U} = -\frac{\mu}{K}\mathbf{V} + \rho_0 (1 - \beta (T - T_{ref}))\mathbf{g} + \mathbf{J} \times \mathbf{B} \tag{4}$$

where **J** is the current density, **B** is the azimuthal magnetic flux density. The gravity force is the sum of inertia force and buoyancy force [16], **g** is gravity constant, T_{ref} is the reference temperature taken as the solidus temperature of the alloy.
In equation (3), c_p^{eq} is the equivalent specific heat, which is introduced to take into account of the latent heat of fusion ΔH_f and f_L is the liquid fraction, assumed to vary linearly with the temperature in the mushy zone expressed as follows equation (6). S_T is the volume heat production and is equal to the Joules heating due to the flow of current.

$$c_p^{eq} = c_p + \rho \Delta H_f \frac{df_L}{dt} \tag{5}$$

$$f_L = \begin{cases} 1 & T > T_L \\ \dfrac{T - T_s}{T_L - T_s} & T_s \geq T \geq T_L \\ 0 & T < T_s \end{cases} \tag{6}$$

The flow of current through the weld pool will give rise to the electromagnetic force. The velocity distribution of the weld pool is affected by these forces. For the calculation of these electromagnetic forces, the following set of equation is adopted in the current study [5].

Current continuity equation

$$\frac{1}{r}\frac{\partial}{\partial r}\left(r\sigma \frac{\partial \phi}{\partial r}\right) + \frac{\partial}{\partial z}\left(\sigma \frac{\partial \phi}{\partial z}\right) = 0 \tag{7}$$

Ohm's Law

$$j_r = -\sigma \frac{\partial \phi}{\partial r} \qquad j_z = -\sigma \frac{\partial \phi}{\partial z} \tag{8}$$

Ampere circumfluence law

$$B_\theta = \frac{\mu_0}{r} \int_0^r r j_z dr \tag{9}$$

Where, σ_E is electrical conductivity, ϕ electrical potential, j_r and j_z are radial and axial current density respectively, B_θ self-induced magnetic field intensity and $\mu_0 = 4\pi \times 10^{-7}$H/m the permeability of vacuum.

1.2 Computational domain and boundary conditions

The computational model used for the finite element analysis was modified to investigate the transient, two-dimensional heat and fluid flow problem for the static TIG welding. Figure 2 shows the computational domain used for the numerical study.

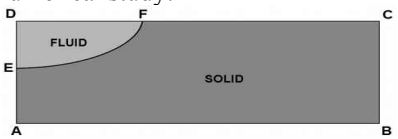

Figure 2: Computational domain for the finite element problem

The geometry includes two sub domains such as a solid domain (ABCFE) and a fluid domain (DEF). The electromagnetic and energy equations were solved in both domains, but the momentum and mass conservation equations were solved only in the fluid domain because the fluid flow takes place only within the fusion region and also to reduce the computational time. A finer mesh size is adopted for the fluid domain and in particular the top surface (DF) where the high gradient occurs [16]. The different boundary conditions for electromagnetic field, temperature and velocity are given in Table 1.

Table 1: Estimated parameters for the IHTP solved with ideal input data.

Boundary	Temperature (T)	Electric potential (ϕ)	Velocity (u, v)
DF and FC	$q_n(r) = -k\frac{\partial T}{\partial n} = \frac{dU_w I_w \eta}{\pi r_H^2}$ e	$j_n(r) = -\sigma\frac{\partial \phi}{\partial n} = \frac{dI}{\pi r_J^2}$ exp	$-\mu\frac{\partial V_s}{\partial n} = \tau_a + \frac{d\gamma}{dT}\frac{\partial}{}$
BC	$-k\frac{\partial T}{\partial r} = h(T - T_0) + \varepsilon\sigma(T^4 \cdot$	$\frac{\partial \phi}{\partial r} = 0$	–
AB	$-k\frac{\partial T}{\partial r} = h(T - T_0) + \varepsilon\sigma(T^4 \cdot$	$\phi = 0$	–
AE and ED	$-k\frac{\partial T}{\partial r} = 0$	$\frac{\partial \phi}{\partial r} = 0$	$\frac{\partial u}{\partial z} = 0, \frac{\partial v}{\partial r} = 0$

Where $j_n(r)$, $q_n(r)$ and τ_a are respectively the current density, heat flux and arc drag force acting at the top surface of the work piece and assumed as Gaussian distributions. The Gaussian current density distribution parameter is calculated from an emperical equation obtained from [18]; $r_J = 0.5342.I^{0.2684}$. where r_J is in *millimiter* and I is in *amper*. The Gaussian heat input was defined by the arc power and the Gaussian heat distribution parameters. For the current study, the instantaneous power calculated as the product of simultaneous current and voltage samples from the experimental data. The parameters of Gaussian distributions are the heat distribution factor $d = 0.5$ (for GTAW), the efficiency $\eta = 0.68$ and the base radius r_H is taken as 3 mm for a current I_w of 150 A and an arc length of 2.4 mm (or $U_w \approx 10.4V$) [16]. Also h is the convective heat transfer coefficient, ε is the emissivity, σ is Stefan-Boltzmann constant and T_0 the ambient temperature.

The temperature dependent surface tension gradient for binary iron-sulfur system, where sulfur is the surface active element, is obtained from the Sahoo et al. [17] relationship.

The constants used in the equations are given in Table 2.

Table 2: Material properties used for the MTHD simulation

Symbol	Material Property	Value
As	Activity of sulphur	0.003 wt%
k_s	Thermal conductivity of solid	26 W/mK
k_l	Thermal conductivity of liquid	20 W/mK
cp_s	Specific heat of solid	486 J/kgK
cp_l	Specific heat of liquid	650 J/kgK
ρ_s	Density of solid	7500 kg/m^3
ρ_l	Density of liquid	6350 kg/m^3
μ	Dynamic viscosity	2.5×10^{-3} kgm^{-1}s^{-1}
β_0	Volumetric expansion coefficient	1×10^{-4} K^{-1}
T_s	Solidus temperature	1673 K
T_l	Liquidus Temperature	1723K

1.3 Numerical Results

Comsol Multiphysics© is used to solve the MTHD problem. This finite element software solves the coupled partial differential equations governing the physical phenomenon. In the current problem the electromagnetic field is first solved and the Lorentz force is calculated for the fluid domain. The Lorentz force will be given as an input to solve the Navier-Stokes equations. Finally the solution gives the electromagnetic, velocity and temperature fields in the domain. A finer mesh size is used in the fluid domain (about 100 µm) and a very fine mesh (about 50 µm) is used on the top boundary where the high gradient occurs. A fixed grid numerical method is used in the model to track the liquid/solid interface. In this method, the computational mesh is generated only once, and the liquid/solid interface is located using the liquid fraction $f_L(T)$ [16]. The time-dependent solver is used. The simulation duration is 6 s. The initial temperature was 293K. The mesh grid is made of triangular finite element using a 2nd order polynomial for temperature and velocity and 1st order polynomial for pressure. This leads to *11574* degrees of freedom. The step time is chosen by the software with a maximum value set to *0.05s*. A time dependent solver using the generalized alpha method was employed (default solver for fluid mechanics). The computation time was about *30mn* on windows® 7 64bits desktop computer with 4 microprocessors (2GHz) and 4 GB memory.

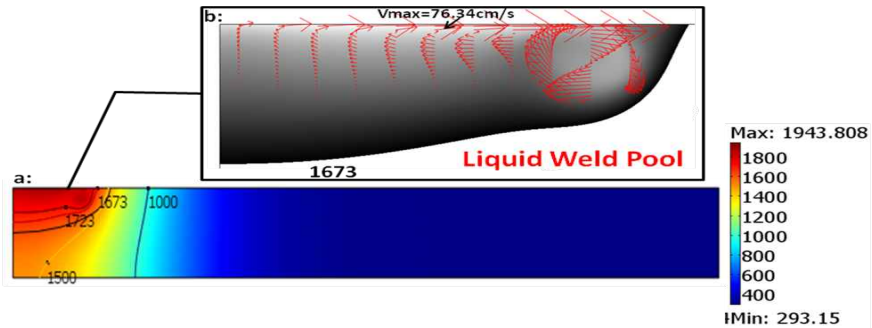

Figure 3: Solution of the forward problem; **a**: Surface temperature distribution and the contour plot **b:**weld pool region and the distribution of velocity

Figure 3 shows the temperature and velocity distribution in the work piece by considering all the driving forces. These results were obtained for an arc current of 150A and arc length of 2.4 mm. The shape of weld pool concluded that the combined effect of arc drag and Marangoni driven flow dominated in the liquid convection resulted in a wider and shallow weld pool shape. The maximum velocity in the weld pool is obtained as 76.34 cm/s.

2. Inverse Heat Transfer Problem (IHTP)

Inverse heat transfer problems are known to be ill posed [15] in contrast to the direct heat transfer problems which are well posed. In this latter, the solution exists, the solution is unique and the solution is stable to small changes in the input data. To deal with these difficulties the inverse problem is usually solved as an optimization problem with regularization. The final goal of the optimization problem for the current study is to determine the uncertain parameters that used in the heat source distribution. Several inverse techniques were used in the past to solve the welding optimization problem: Levenberg-Marquardt [11, 13], gold section [12] and gradient conjugate with adjoint method [14]. For the present study a damped least square optimization technique named Levenberg-Marquardt method is used. It is a combination of Gauss Newton algorithm and steepest decent technique [15].

2.1 Levenberg Marquardt Algorithm

The Levenberg-Marquardt method has been widely used in various inverse heat transfer problems [11, 13]. It involves the minimization of an objective function which depicts the difference between the computed and measured values.

$$S(\overline{p}) = \left[Y_i - T_i\right]^T W_1 \left[Y_i - T_i\right] + \left[\Gamma_i - D_i\right]^T W_2 \left[\Gamma_i - D_i\right] \tag{12}$$

Where Y_i are the measured temperatures, T_i the calculated temperatures and Γ_i and D_i are the measured and calculated weld pool width at point x_i, $i=1\ldots n_s$. The subscript T denotes the transpose: $\left[Y_i - T_i\right]^T = \left[Y_1 - T_1, \ldots, Y_{n_S} - T_{n_S}\right]$.The Levenberg-Marquardt method associated to an iterative process leads to estimate the unknown vector $\overline{P}$ at iteration $k+1$ as follows:

$$\overline{p}^{k+1} = \overline{p}^k + \left[J_1^{kT} W_1 J_1^k + \lambda^k \Omega^k\right]^{-1} \left[J_1^{kT} W_1 \left(T_i - Y_i\right)\right] + \left[J_2^{kT} W_2 J_2^k + \lambda^k \Omega^k\right]^{-1} \left[J_2^{kT} W_2 \left(\Gamma_i - D_i\right)\right] \tag{13}$$

Where $J(\overline{p})$ is the sensitivity matrix which is defined as the transpose of the term $\left[\partial T_i\ (\overline{p}) / \partial p\right]$. The elements of the sensitivity matrix are called the sensitivity coefficients. The sensitivity coefficient is thus defined as the first derivative of the estimated temperature with respect to the unknown parameters $\overline{p} = \left\{\eta, R_{B1}, R_{B2}\right\}$. λ^k is positive scalar which is introduced to alleviate that matrix $J^T J \approx 0$ is ill-conditioned near the initial guess used for the unknown parameters. Ω^k is a diagonal matrix. The term $\lambda^k\Omega^k$ damps oscillations and instabilities due to the ill-conditioned character of the problem. This damping parameter is large at the beginning of the iterative procedure (and the method is like the steepest descent method) then it decreases when the procedure advances to the solution (and the method tends to the Gauss method). W is a diagonal matrix where the diagonal elements are given by the inverse of the standard deviation of the measurement errors.

The Levenberg-Marquardt algorithm is presented in figure 4. We chose an initial set of parameters $\overline{p}^0 = \left\{\eta, R_{B1}, R_{B2}\right\}$ and an initial value for the damping parameter $\lambda^0=0.001$. The iteration number is initialized ($k=0$).

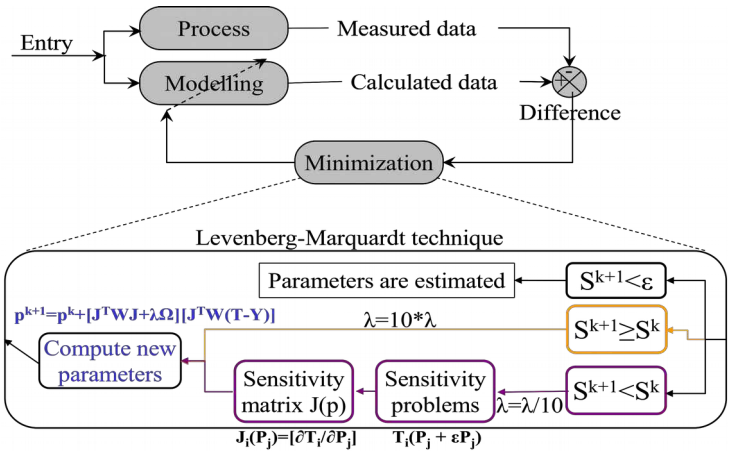

Figure 4: the Levenberg-Marquardt method for the parameter estimation.

The keystone of the Levenberg-Marquardt method resides in the sensitivity matrix coefficients. These sensitivity coefficients must be linearly independent or the problem is over-parameterized. The next paragraph will deal with the analysis of these sensitivity coefficients in order to verify the relevance of the measured data for solving our inverse heat transfer problem.

3. Numerical inverse analysis and discussion

3.1 Definition of the Parameter to estimate

The arc plasma effect on the work piece is modelled with the Gaussian heat distribution $\phi(r, t)$, which include the instantaneous current and voltage data (U_w, I_w) from the experimental measurement and is represented as follows;

$$\Phi\left(Uw, Iw, r_b, \eta\right) = \eta \frac{1}{2} \frac{Uw(t).Iw(t)}{\pi R_b^2} e^{-\frac{1}{2}\left(\frac{r}{R_b}\right)^2} \tag{14}$$

The investigated parameters are the GTAW efficiency η and Gaussian radius R_B as they are the parameters of the heat flux that are unknown. They parameters affect the temperature field along the simulation and the weld pool growth. Moreover, we propose that the Gaussian radius R_B varies linearly with regards to the time variable t, and is given as follows:

$$R_B(t) = \frac{R_B(t_f) - R_B(t_0)}{\Delta t}.t + R_B(t_0) \tag{15}$$

In order to represents the "transient" radius of the arc plasma at the ignition of the electrical arc. Finally the vector $\overline{P}$ is equal to $\overline{p} = \left\{\eta, R_B^{t_0}, R_B^{t_f}\right\}$ hence 3 unknown parameters to estimate.
In this work, a numerical differentiation based on a forward difference scheme has been used [15] in order to calculate the required coefficients of the sensitivity matrix.

3.2 Numerical Inverse Analysis with ideal data

First, the IHTP is solved with ideal input data in order to check that the inverse program converges towards the given set of parameters with a good accuracy. The ideal input data are obtained by solving first the direct problem (equations (1) to (9)) with the following values: $\eta=0.68$, $R_{B1}=2.7$ *mm* & $R_{B2}=3.2$ *mm.* This simulation gives us ideal (or reference) data about time evolution of both temperature and weld pool radius. These data are called "ideal" as there is no measurement error. The initial values

used for the three parameters are: η*=0.2,* R_{B1}*=20 mm &* R_{B2}*=20 mm* at the first iteration of the IHTP. The positions of the thermal sensors were chosen on the back side at radii 4mm (sensor 1) and 8mm (sensor 2).

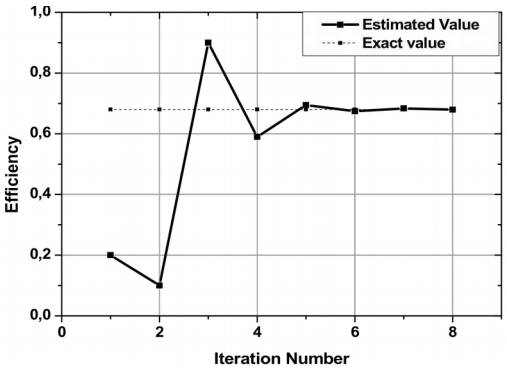

Figure 5: Estimated efficiency along the iteration process.

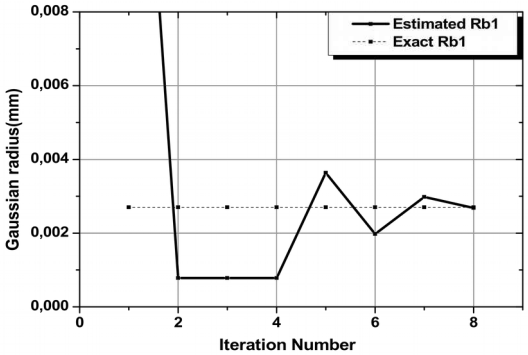

Figure 6: Estimated Gaussian radius Rb_1 along the iteration process.

Figure 5, 6 and 7 shows the estimated parameters along the iterative process. The three parameters are perfectly estimated at the final iteration 8. The final values are reported in table 3. The error on the three estimated parameters is below 0.08%. The residual error is due to numerical noise. Figure 8 presents the evolution of the objective function along the iterative process. The initial value of the objective function was $1.9x10^7$ and decreased in 8 iterations to the final value of 17.67 which is quite close to zero as expected.

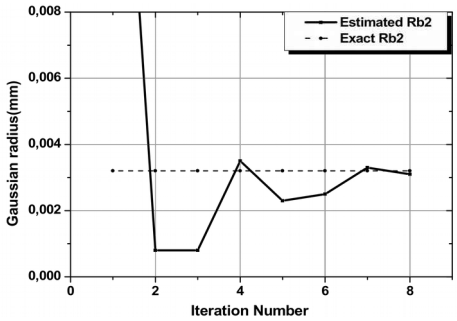

Figure 7: Estimated Gaussian radius Rb_2 along the iteration process.

Figure 8: Evolution of the objective function along the iteration process

Table 3: Estimated parameters for the IHTP solved with ideal input data.

Parameters	Exact value	estimated	% error
η	0.68	0.6799	0.015
R_{B1} (mm)	2.7	2.68	0.08
R_{B2} (mm)	3.2	3.1	0.086

3.3 Numerical Inverse Analysis with noised input data

The goal of this numerical work is to evaluate the ability of the inverse algorithm to estimate the three unknown parameters with regards to measurement errors. Two sorts of measurement errors are investigated: the first is due to the thermocouple itself and the acquisition device while the second is due

to the thermocouples position inaccuracy. For the first case, a random measurement error is added to the reference temperature with a maximum standard deviation σ(t) of 5% of the actual temperature (e.g: $|\sigma(t)| \leq 5\% \times T_{REF}(t)$ so the new inputs for the IHTP were: $T_{NOISE}(t)=T_{REF}(t)+\sigma(t)$). An inaccuracy of ±0.5mm is assumed on the thermocouple position for the second case. So the reference data were made at r=3.7mm and r=8.3mm for sensors 1 and 2 respectively. The IHTP was solved by assuming that the sensors position was 6mm and 8mm. The final results are presented in table 4.

Table 4: Parameters estimated for the three studied cases of error.

Parameters	Exact values	Case 1 (at 9th iteration)		Case 2 (at 9th iteration)	
		Estimated	Error (%)	Estimated	Error (%)
η	0.68	0.683	≤0.44	0.73	≤7.4
R_{B1} (mm)	2.5	2.538	≤1.5	2.623	≤4.9
R_{B2} (mm)	3.5	3.438	≤1.78	4.028	≤15.1
Heat flux integral	1.425×10^5	1.434×10^5	≤0.63	1.386×10^5	≤2.7
Final objective funciton		35481.3		10836.8	

Both studied cases converged to a limit value for the objective function. The final objective function for case 1 is 3 three more important than the one for case 2. The same number of thermocouples and time steps are used in these two studies. Parameters estimated with errors on thermocouple position seemed to lead to good results according to the objective function. Indeed, the value of the three estimated parameter are really far than the one expected: $\eta=0.68$, $R_{B1}=2.7$ *mm* & $R_{B2}=3.2$ *mm*. the biggest error is made on the estimation of R_{B2} with 15% error followed on GTAW efficiency with 7.4% error. A small error on thermocouple position within ±0.5mm leads to wrong estimates. The integral of the heat flux over the space and time interval was computed for both cases. The heat flux integral is below 3% error for the second case despite the estimated parameters. For measurement errors due to the acquisition chain, the three parameters are very well estimated as well as the heat flux integral despite the final objective function value. In this case, the Levenberg-Marquardt filtered the noised on input data and finally led to a good estimation of the parameters.

3.4 Discussion

Three numerical cases were studied previously:

1. resolution of the IHTP with "ideal" data (without any measurement error in the input data);
2. resolution of the IHTP with "realistic" data (including only measurement errors due to the acquisition chain);
3. Resolution of the IHTP with "ideal" data but the thermocouple position was known with certain accuracy.

The case with ideal input data demonstrated that the developed inverse problem was able to estimate the three parameters with an excellent accuracy. The residual objective function is close to zero (17.7) in comparison to its initial value about 1.9×10^7. This residual is assumed due to the numerical error of the FEM software. The GTAW efficiency parameter is the first to be estimated correctly after 5 iterations, figure 5, while it takes to 7/8 iterations for the Gaussian radii to be estimated correctly, figure 6 and 7. Indeed, the temperature field is very sensitive to the GTAW efficiency parameter. A small change in this parameter generates important changes in the temperature field and weld pool dimensions.
The two other cases studied the effect of two kinds of error on the estimation of the parameters. The error due to the acquisition chain, about 5% of the reference temperature, was a realistic error. This error led finally to a very good estimation of the parameters. Actually, the Levenberg-Marquardt technique has filtered off the perturbation added on the reference data. It converged toward the right parameters with accuracy below 2% on Gaussian radii and below 0.5% on GTAW efficiency. The Levenberg-Marquardt

is quite robust to such measurement noise if it is random and distributed with a normal law. Such noise measurement does not prevent any estimation of the three parameters. This conclusion does not mean that the error due to the acquisition chain can be neglected. Conversely, small errors on the thermocouple position (within ±0.5mm as the thermocouple size is 0.5mm) leads to wrong values for the three parameters. In the studied case, GTAW efficiency is overestimated as the input data was calculated closer to the centre (3.7mm) while the temperature was computed at 4mm in the IHTP. The second Gaussian radius was also wrongly estimated: 4mm instead of 3.2mm. This probably due to the error on the position of the second thermocouple: the IHTP used 8mm while it was 8.3mm for obtaining the input data. The energy is spread over a large area. Despite these wrong estimated values, the method leads to a fair estimation of the heat flux integral with an error below 3%.
Finally, reasonable measurement noise due to the acquisition chain does not prevent the estimation of the three parameters while errors on thermocouple position prevent any accurate estimation of these parameters but it gives a fair idea of the energy absorbed by the work piece during a static GTA welding spot. The stated IHTP can be solved with experimental data as the method is robust to noise measurement. A great care must be done on the position of the thermocouple in order to get a good estimation of the three parameters.

4. Conclusion

A GTAW modelling was established in order to describe a stationary GTA welding experiment. This modelling includes coupling and simultaneous solution of electric potential, heat transfer and Navier-Stokes equations. In this paper, an inverse heat transfer problem has been stated in order to estimate heat flux parameters. The parameter estimation was carried out for several numerical test cases: ideal input data (without any measurement errors) and more realistic input data (including two sorts of errors). The temperature measurement were made on the disc backside as the topside is almost impossible to instrument due to the severe electric and radiating conditions of the arc welding process. The inverse thermo convective model developed was able to get back the parameters with reasonable accuracy for the ideal test case and the test case including noise measurement in the input data. For the third test case, the errors were supposed on the sensor position. This case led to wrong estimated parameters but provided a good knowledge of the heat absorbed into the work-piece. The Levenberg-Marquardt technique is robust to measurement errors as it filters off the noise in the input data. The thermocouple must be positioned carefully as the result of the IHTP depends strongly on the accuracy of their position. The experimental data will be shortly used for solving the inverse heat transfer problem.

References

1. G. M. Oreper, T. W. Eagar and J. Szekely, Convection in arc weld pools, *Welding Research Suppliment,* 307s-312s, 1983.
2. S. Kou and D. K. Sun, Fluid flow and weld penetration in stationary arc welds. *Metallurgical and Material Transactions A*, 16A, 203-213, 1985.
3. A. Matsunawa, S. Yokoya and Y. Asako, Convection in weld pool and its effect on penetration shape in stationary arc welds, Transactions of JWRI, Welding Research Institute of Osaka University, Japan, Vol:16, No.2, 229-236, 1987.
4. R. Natarajan, A. Seppo and A. Korpela, Fluid dynamics of a stationary weld pool, Metallurgical Transactions A, 21A, 45-57, 1990.
5. H.G. Fan, H.L. Tsai, S.J. Na. Heat transfer and fluid flow in a partially or fully penetrated weld pool in gas tungsten arc welding, *International Journal of Heat and Mass Transfer*, 44 (2001) 417-428.
6. M. Tanaka and J. J. Lowke, *Topical Review:Predictions of weld pool profile using plasma physics*, Journal of Physics D: Applied Physics, 40, R1-R23, 2007.
7. D. Rosenthal, The theory of moving source of heat and its application to metal transfer, Trans. ASME, Vol.43 no.11, 1946.
8. V. Pavelic, R. Tanbakuchi and O. Auyehara, Experimental and computed temperature histories in gas tungsten arc welding of thin plates, Welding Journal Research Suppliment, 48 (7): 295s-305s, 1969.

9. J. A. Goldak, A. P. Chakravarti, and M. Bibby, A new finite element model for welding heat sources, Metallurgical Transactions B, 15, 299-305, 1984.
10. N. S. Tsai and T. W. Eagar, Distribution of heat and current fluxes in Gas Tungsten Arcs, Metallugical Transactions B, **16B**, 841-846 (1985).
11. A. De, T. DebRoy. Improving reliability of heat and fluid flow calculation during conduction mode laser spot welding by multivariable optimisation; Science and Technology of Welding and Joining (2006) (11) 143-153.
12. C.V. Goncalves, L.O. Vilarinho, A. Scotti, G. Guimaraes. Estimation of heat source and thermal efficiency in GTAW process by using inverse techniques. Journal of Materials Processing Technology 172 (2006) 42–51.
13. S. Rouquette, J. Guo, P. Le Masson. Estimation of the parameters of a Gaussian heat source by the Levenberg–Marquardt method: Application to the electron beam welding. International Journal of Thermal Sciences 46 (2007) 128–138.
14. M. Dal, P. Le Masson, M. Carin. Estimation of fusion front in 2D axisymmetric welding using inverse method. International Journal of Thermal Sciences 55 (2012) 60-68.
15. Ozisik N. M., and Helcio R. B. Orlande, **'**Inverse heat transfer fundamentals and applications', Taylor and Francis, New York, 2000.
16. A. Traidia: 'Multiphysics modelling and numerical simulation of GTA weld pools', *PhD thesis*, Ecole Polytechnique, ENSTA UME-MS, Paris, 2011.
17. P. Sahoo, T. Debroy, M. T. McNallan, Surface tension of binary metal surface active solute systems under conditions relevant to welding metallurgy, Metallurgical Transactions B, 19, 483-491, 1988.
18. M.S. Min Hyun Cho : 'Numerical simulation of arc welding process and its application', PhD thesis, The Ohio State University, 2006.